Rare Met. (2021) 40(11):3279–3288
https://doi.org/10.1007/s12598-020-01671-3

RARE METALS

ORIGINAL ARTICLE

Nano-yttrium-containing precipitates of T6 heat-treated A356.2 alloy when trace yttrium (Y less than 0.100 wt%) added

Xin-Ping Hu*, Qing Wang, Henry Hu, Rui-Xin Li, Yang Zhao, Zhi-Ming Wang, Bing-Rong Zhang

Received: 3 April 2020 / Revised: 14 May 2020 / Accepted: 1 December 2020 / Published online: 6 February 2021

Abstract To investigate the effect of yttrium (Y) on microstructure refinement and mechanical properties of aluminum alloy A356.2, the different trace contents of Y (0 wt%, 0.025 wt%, 0.050 wt%, 0.075 wt%, or 0.100 wt%) were introduced into the liquid alloy. The alloys were fabricated in a preheated permanent mold, and subsequently treated by a T6 heat treatment. The results of tensile testing indicate that the yield strength (YS), the ultimate tensile strength (UTS) and the elongation (El) of the A356.2 alloy are improved by the Y additions. The YS dependence on grain size for the test alloys follows the Hall–Petch equation, which gives $YS = -354.1 + 2875.2d^{-1/2}$ with a correlation of $R^2 = 0.83$. As 0.050 wt% Y is added, the optimum values of the YS, UTS and El are achieved after T6 heat treatment. The secondary phases were identified by X-ray diffraction (XRD) which mainly consisted as Si, Mg_2Si and Al_3Y. The scanning electron microscope (SEM) and energy-dispersive spectrometer (EDS) analyses reveal the presence of the nano-sized Al_3Y particles on the surface of the Si phase. The A356.2 alloy with the Y addition is strengthened by the dendritic refinement, and the presence of the micron- and nano-sized Al_3Y precipitates.

Keywords Yttrium; Microstructures; Mechanical properties; T6 heat treatment; A356.2 alloy

X.-P. Hu*, Q. Wang, R.-X. Li, Y. Zhao, Z.-M. Wang, B.-R. Zhang
School of Mechanical and Automotive Engineering, Qilu University of Technology, Jinan 250353, China
e-mail: huxxpp@qlu.edu.cn

H. Hu
Department of Mechanical, University of Windsor, Automotive & Materials, Engineering Windsor N9B 3P4, Canada

1 Introduction

A356 is a hypoeutectic Al-Si alloy which has been widely employed to manufacture various parts used in the aerospace and automotive industries. Due to the excellent castability, the components are often made by permanent mold casting process, of which the solidification rate is relatively low. As-cast A356 alloy contains coarse eutectic Si phases with flake and needle-like shapes which cause stress concentration during mechanical loading and downgrade the mechanical properties. To increase its strengths, efforts of introducing foreign reinforcements in the as-cast alloys are attempted [1–3]. The introduction of foreign reinforcements increases both materials and manufacturing costs. Modification of eutectic Si phases with small amounts of alloying additives, precipitation hardening by heat treatment, and refinement of primary α-Al phase appear to be the cost-effective approaches for improvement of mechanical properties of the hypoeutectic alloys [4, 5]. It has been demonstrated that light rare earth elements (RE) such as La [6, 7], Ce [8, 9], Pr, Sm [10], as well as heavy rare earth element Gd [11] are capable of modifying not only primary Si phases but also the shape of eutectic Si. Among the La, Sm, Pr and Ce, Ce has the large negative mixing enthalpies with Si, and shows the best effect on the modification of eutectic Si phase [12]. With minor addition of Mg around 0.3 wt%, precipitation hardening takes place during heat treatment of hypoeutectic Al–Si–Mg alloys, in which strengthening phase Mg_2Si forms. The previous studies [13–16] indicate that, within the same group of Ce in the periodic table, elements yttrium (Y) or scandium (Sc) can modify eutectic Si phases, refine primary α-Al phases and/or accelerate the precipitation kinetics. These effects co-occur when Y is added to both the hypoeutectic Al–Si–Mg alloy [13, 16] and

hypereutectic Al-20Si alloy [15]. Rao et al. [17] reported the microstructural refinement of as-cast A356 alloy obtained by melt inoculant with a master alloy of Sr (modifier), Sb (modifier) and Al-Ti-C (grain refiner). Zhang et al. [18] enhanced the strength and ductility of A356 alloy by rapid solidification and thermo-mechanical treatment. The study by Mahmoud et al. [19] indicated that the addition of large amounts of rare earth elements Ce and La (2 wt%) causes a marked increase in the freezing zone coupled with a marked volume fraction of RE-based intermetallics which reduce the alloy feedability and lead to the formation of a significant percentage of shrinkage porosity in the as-cast A356. The situation is more severe in Sr-treated alloy A356.

Yttrium is demonstrated to be an excellent modifier and refiner for the Al-Si alloys. Liu and Hu [13] examined the refinement of primary α-Al phases in a semi-solid A356 alloy with the Y addition of 0.3–0.8 wt%. Dong et al. [16] characterized the microstructure of the metallic mold-cast and T6 heat-treated A356 alloy modified by Sr (0.04 wt%) and Y (0.3 wt%). The Sr and Y additions promote the formation of Al_3Y phase and increase the nucleation rate of primary α-Al phases. Moreover, the additions of Sr and Y change the shape of eutectic Si phases to fine granules from coarse needles and flakes. The amount of Y addition to A356 alloy appears relatively high in the past studies. Since yttrium is scarce and expensive, the minimization of Y usage without sacrificing its beneficial effects on microstructure is essential for the industry to adopt Y in aluminum alloys. Till now, there are limited studies on Y addition to A356 alloy, notably at a microalloying level of up to 0.100 wt%. Therefore, the effect of Y microalloying at a trace amount on microstructural refinement and phase constituents in relation to mechanical properties needs to be investigated.

2 Experimental

The commercial A356.2 alloy was selected as matrix and its main chemical compositions used are 6.803 wt% Si, 0.230 wt% Mg, 0.147 wt% Ti, 0.069 wt% Fe and balance Al. The Al-0.100 wt% Y master alloy wrapped in aluminum foil was added into the melt to prepare the alloys with various contents of Y. Five groups of samples with different contents of Y were designed, and the alloys with different Y contents (0 wt%, 0.025 wt%, 0.050 wt%, 0.075 wt% and 0.100 wt%) are labeled as Y000, Y025, Y050, Y075 and Y100, respectively. A 5-kW electrical resistance furnace and a graphite crucible were chosen to prepare the alloys. The prepared alloys were preheated at 300 °C for 2 h and then gradually heated up to 750 °C. The melts were then deslagged and poured into the prepared permanent mold (270 °C) with the pouring temperature of 650 °C. To evaluate the tensile properties, the round tensile specimens shown in Fig. 1 were manufactured. The detail of equipment can be seen in Ref. [20].

The specimens to be investigated were divided into two groups which are in as-cast and T6 heat-treated conditions. Tensile test and microstructure analysis were then conducted to the well-prepared samples. T6 heat treatment was carried out in anti-oxidation atmosphere furnace (TCXQ-1700). The T6 heat treatment started with solution treated at 530 °C for 8 h, followed by quenching in water with 25 °C and then artificial aged at 150 °C for 3 h. All specimens were tested on a 100-kN universal tensile testing machine (CHT4605) at a load speed less than 1 $mm \cdot min^{-1}$ at room temperature to obtain ultimate tensile strength (UTS), yield strength (YS) and elongation (El). In order to avoid the effect of tensile tests on microstructures, the samples for microstructure analysis were cut from where at least 5 mm away from the fracture. Individual samples for microstructure analysis were prepared by standard mechanical polishing and then etched by Keller reagent (95.0 ml H_2O + 2.5 ml HNO_3 + 1.5 ml HCl + 1.0 ml HF) for 30 s. A Leica DM2700M optical microscope (OM) was used to observe the distribution and morphologies of Si, Mg_2Si, α-Al and Al_3Y in A356 with different Y additions. The secondary dendrite arm spacing (SDAS) and the grain size were measured and calculated with the help of image processing software. The microstructure images were captured by SUPRA^{TM} 55 thermal field emission scanning electron microscope (FESEM) equipped with an energy-dispersive spectroscope (EDS) device. The Brinell hardness is tested by an XHB-3000 hardness tester with a 5 mm diameter cemented carbide ball under a load of 1250 N for 30 s. Differential scanning calorimetry (DSC) was carried out by using high temperature differential scanning calorimeter (DSC 404 F3) with Ar as protective gas. The phases were also determined by X-ray diffraction (XRD, Rigaku RINT-2000).

3 Results and discussion

3.1 Microstructures of as-cast and T6 heat-treated samples

Figure 2a, b depicts typical OM and SEM images of the as-cast A356.2 alloy. Figure 2c, d represents typical OM and SEM images of the T6 heat-treated A356.2 alloy. They were selected from the images of microstructures of A356.2 with different trace contents of yttrium (0 wt%, 0.025 wt%, 0.050 wt%, 0.075 wt%, or 0.100 wt%), and the content of yttrium here is 0.075 wt%. There are two different phases in OM images, one is α-Al matrix and

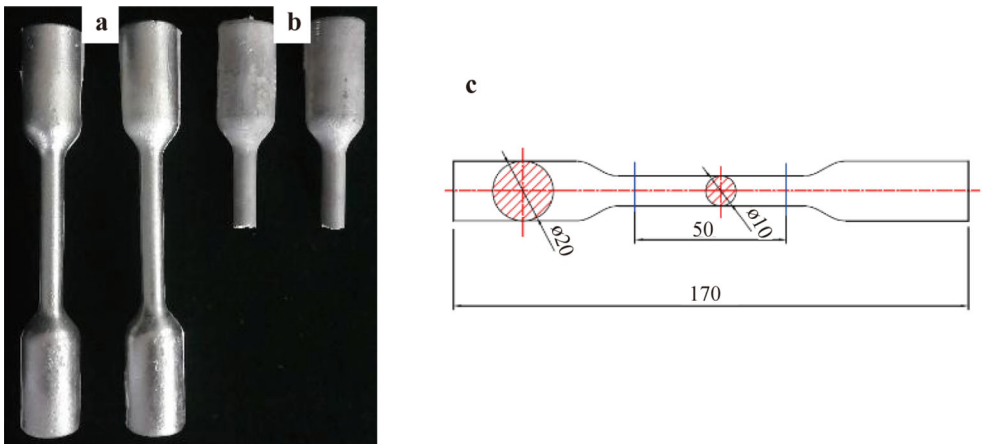

Fig. 1 Round tensile specimens: **a** before tensile test, **b** after tensile test and **c** AutoCAD technical drawing (mm)

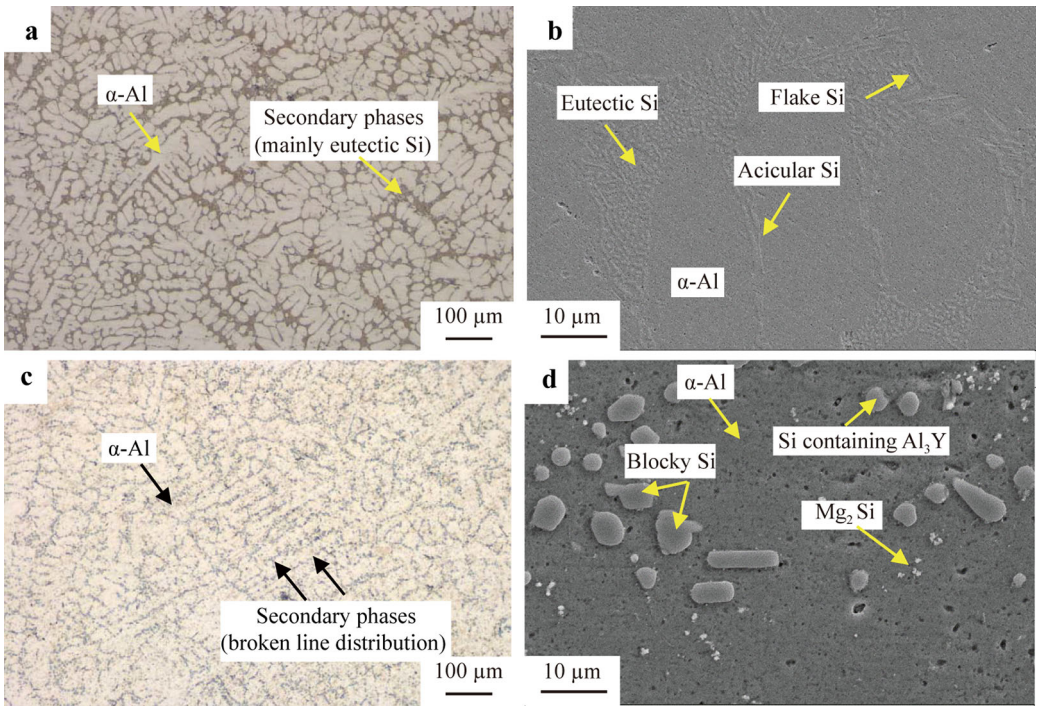

Fig. 2 **a** OM and **b** SEM images of as-cast A356.2 alloy; **c** OM and **d** SEM images of T6 heat-treated A356.2 alloy

another is secondary phases (mainly eutectic Si). The morphology of Si in as-cast alloy is typical flake and long acicular shapes. After T6 heat treatment, the long acicular Si can be rarely found, instead, the small bulk Si and little Mg_2Si particles appear in the boundary of α-Al grains. The α-Al grain size and their secondary dendrite arm spacing (λ_2) of all the microstructures of A356.2 with different Y additions are concluded in Fig. 3.

It could be seen that Y plays a refining role on the microstructures of α-Al grains. Y is active and could be dissolved easily in liquid aluminum. At high temperatures, it reduces the surface energy and surface tension of the interfaces between old and new phases, and then decreases the nucleation power of the phase transformation. This helps to prevent grain growth and generate large number of heterogeneous nucleation substrate. As a result, the microstructures of the α-Al and Si phases are all refined.

On the other hand, Y could interact with other elements to strengthen A356.2 alloy with the formation of intermetallic compounds such as Al_3Y. High melting point Al_3Y is hexagonal with Ni_3Sn-type structure, which is mainly precipitated at 639 °C by eutectic reaction ($Liquid_{9.5\%Y} \rightarrow \alpha_{Al,0.17\%Y} + \alpha_{Al_3Y}$). On the base of Al-Y phase diagram, Al_2Y is also precipitated at 645 °C by

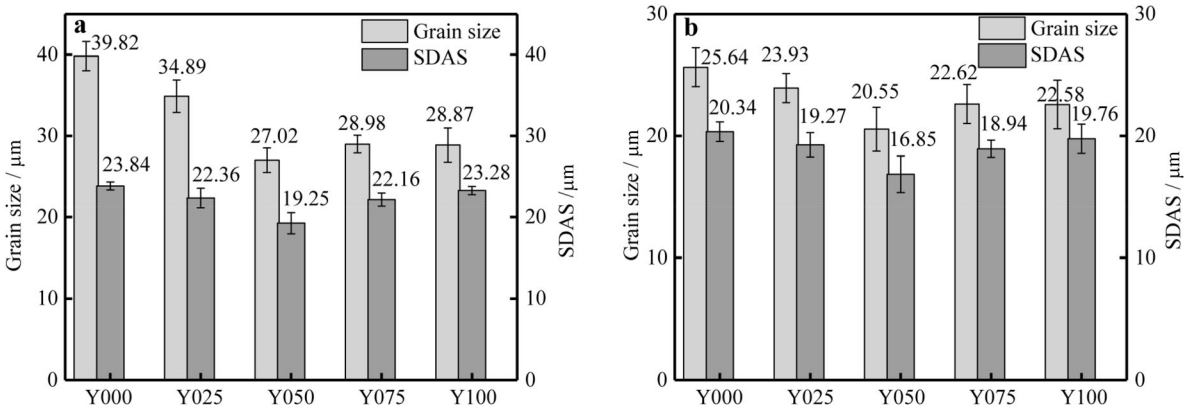

Fig. 3 Grain sizes and SDASs of A356.2 alloys: **a** as-cast and **b** T6 heat treated

eutectic reaction ($\text{Liquid}_{9.5\%Y} \rightarrow \alpha_{Al} + Al_2Y$) [13]. The lattice constant of cubic α-Al is 4.049×10^{-10} m, and one lattice constant of Al_3Y is 4.233×10^{-10} m, so the lattice constant mismatch ($\delta = (a_{Al} - a_{Al_3Y})/a_{Al_3Y} \times 100\%$) is only 4.35%. On the view of dimensions, the solid Al_3Y could be as crystal nucleation base of α-Al during solidification, and refine the α-Al grains.

3.2 Mechanical properties

3.2.1 Tensile test

Figure 4 shows the tensile stress–strain curves of the as-cast and T6 heat-treated A356.2 with the additions of 0 wt%, 0.025 wt%, 0.050 wt%, 0.075 wt% and 0.100 wt% Y, respectively. The UTS of as-cast A356.2 is improved when Y is added, and the best optimized UTS result is from A356.2 with 0.075 wt% Y (Y075), followed by the alloy with 0.050 wt% Y (Y050). After T6 heat treatment, the alloy with the best optimized YS and UTS results is from Y050 (0.050 wt% Y). The YS, UTS and El are concluded in Fig. 5.

Among the five groups of experimental results, it is easy to conclude that the Y050 achieved the optimum values of the YS, UTS and El. Comparing with that of the as-cast Y000, the YS, UTS and El values of as-cast Y075 are increased to 174 MPa, 189 MPa and 7.5%, and improved by 40.32%, 34.04% and 74.42%, respectively. It can be seen from Fig. 5 that the YS and UTS after T6 heat treatment increase significantly, and these five groups' average values increase from 136 and 165.2 MPa to 247.8 and 299.2 MPa comparing with the T6-treated Y000. The YS, UTS and El values of T6-treated Y050 compare to the as-cast Y050 are improved from 95 MPa, 182 MPa, 4.4% to 302 MPa, 322 MPa and 11.2%, and improved by 218%, 77% and 155%, respectively.

3.2.2 Brinell hardness (HB) test

The results of the Brinell hardness of as-cast and T6 heat-treated A356.2 alloys are presented in Fig. 6. It can be seen that the hardness increases after T6 heat treatment, which is attributed to the addition of Y. The larger the amount of Y

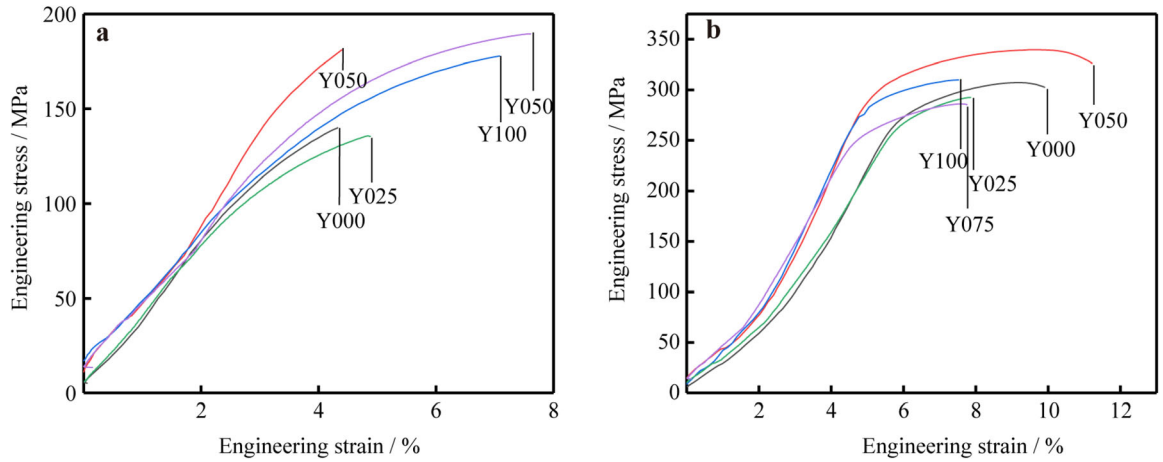

Fig. 4 Representative tensile stress–strain curves of A356.2 specimens: **a** as-cast and **b** T6 heat treated

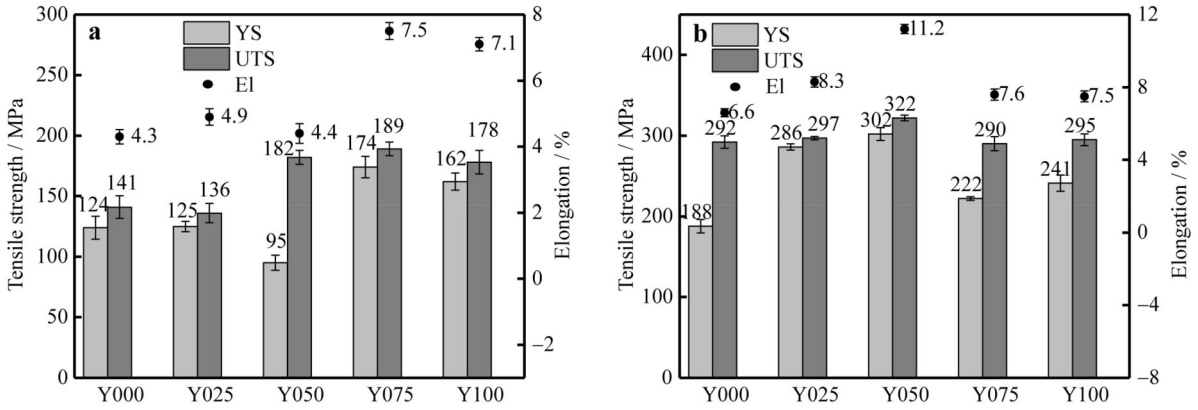

Fig. 5 Tensile strengths of A356.2 specimens: **a** as-cast and **b** T6 heat treated

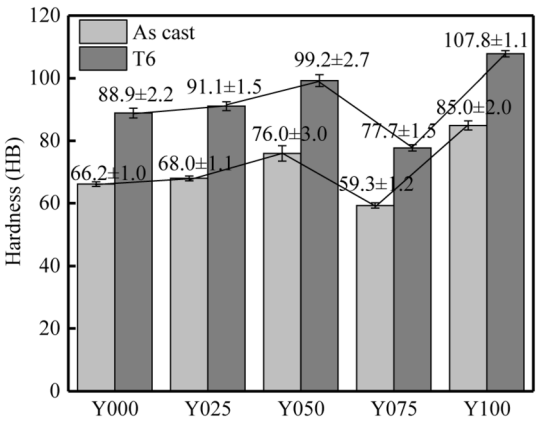

Fig. 6 Hardness test results of as-cast and T6 heat-treated A356.2 alloys

is added, the larger the value of hardness is (Y750 except). The smallest value of hardness of Y750 might be caused by the large grain size of α-Al. In addition, the hardness values of each group keep stable that the fluctuation is less than ± 1.5, and the maximum is ± 3.0.

The effects of Y on mechanical properties of as-cast A356.2 alloy are mainly embodied two factors as below: (1) promoting the α-Al dendrites to equiaxed crystal transformation; (2) hindering the growth of α-Al grains and the eutectic silicon [21, 22]. The atomic radius of Y is 1.74×10^{-10} m, of Al is 1.43×10^{-10} m, which indicate that Y is slightly larger than Al. When Y is dissolved in Al, lattice distortion of α-Al could be induced, and this causes materials solution strengthening. But this takes little strengthening effect, Y is hard to be dissolved in the α-Al matrix [23, 24] due to its low solid solubility in aluminum which is less than 0.03 at%.

The strength of as-cast A356.2 alloy is mainly dominated by grain refinement. It is well known that Hall–Petch equation written below [25] shows the relationship between the yield strength and grain size:

$$\mathrm{YS} = \sigma_0 + Kd^{-1/2} \tag{1}$$

where σ_0 and K are constants, d is the mean measured grain diameter (grain size) shown in Fig. 3. According to the tensile results, the fitting relationship between the yield strength and grain size is $\mathrm{YS} = -371.3 + 2910.3d^{-1/2}$ with a correlation of $R^2 = 0.65$ which is drawn in continuous line in Fig. 7. The fitting result is somewhat not satisfactory. However, noticing that the point (0.192, 95) lies far away from the fitted line, and if it is omitted, the fitting relationship is changed to $\mathrm{YS} = -354.1 + 2875.2d^{-1/2}$ with a correlation of $R^2 = 0.83$ which is drawn in dot line in Fig. 7. It shows a good linear fitting. As shown in the red triangle points lying in right up corner of the figure, it indicates that the YS is improved largely after T6 heat treatment.

After T6 heat treatment, the strength is improved significantly, this could been seen from Figs. 4, 5, and their Brinell hardnesses shown in Fig. 6 are also improved. This should be

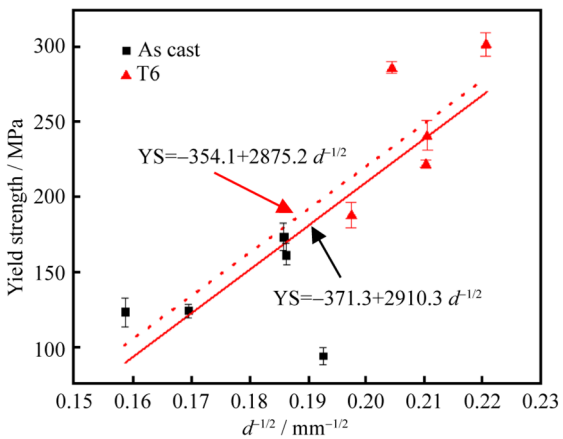

Fig. 7 Linear fit results of Hall–Petch equation between YS and square root of grain diameter ($d^{-1/2}$) of primary α-Al grains. Continuous line is fitting results of all ten points, and dot line is fitting results of nine points except point (0.192, 95) which lies far away from fitted line

mainly due to the T6 effect. When heating and holding at high temperatures, the long needle or flake-like eutectic Si become shorter, even change into particles or tiny bits. The eutectic Si will undergo three stages as: (1) edges rounding, (2) bays occurring, (3) fragmentation and spheroidization. These changes are in accordance with the principle of minimum free energy in thermodynamics and related to the diffusion and dissolution of Si atoms. During quenching process, the broken, fragmented, spheroidized microstructure is remained the same in low temperature atmosphere. In artificial aging stage, its morphology is adjusted, and the stress concentration is released effectively [26].

Mg_2Si and Al_3Y are supersaturated in solid solution, the strengthening mechanism for A356.2 alloy lies in mainly three aspect: (1) grain boundary strengthening, (2) hard particles strengthening, (3) dislocation strengthening [18]. It is well known that Mg_2Si plays an important role in improving the strength of Al-Si alloy. The melting point of pure Mg_2Si is 1085 °C, and the eutectic reaction $Liquid_{1.7\,at\%Si} \rightarrow \alpha_{Mg} + Mg_2Si$ occurs at 637.6 °C according to the Mg-Si phase diagram. In the as-cast A356.2 alloy, undissolved solid Mg_2Si appears in the boundary of α-Al matrix in blocky morphology is shown in Fig. 2a. Actually, it is difficult to distinguish the phase in such secondary phase region in A356 industrial alloy. In the stage of solutionizing in T6 heat treatment, this blocky Mg_2Si becomes smaller and can be partially dissolved. In the stage of artificial aging, some small Mg_2Si particles are precipitated as the solubility decreased in α-Al and Si phase. The undissolved blocky Mg_2Si can be also observed in the fracture surface in Refs. [2, 27].

For Mg_2Si (β phase) in T6 heat-treated A356 alloy, the precipitating sequence is as follows: supersaturated solid solution (SSS) to needle-shaped β″, then to rod-shaped β′, then to plate-shaped β. β″ is Guinier–Preston (GP) zone with cluster of (Mg + Si) spherical atoms before precipitation, β′ is Mg_9Si_5 and is in a semi-coherent relation to the α-Al matrix [28]. Their orientation relationships are $(001)_{\beta'}$ // $(100)_{\alpha\text{-Al}}$ and $[100]_{\beta'}$ // $[011]_{\alpha\text{-Al}}$ [29, 30]. In the fracture of tensile test, some dislocation slip bands are found under SEM. Those hinder the movement of the dislocations, and the strength is improved accordingly [31].

3.3 Phase identification

3.3.1 XRD analysis

XRD analysis was carried out for A356.2 and Y modified alloys to confirm the presence of Mg_2Si and Al_3Y intermetallic phase. Figure 8a shows XRD patterns of as-cast Y000 and Y050 alloys, Fig. 8b is that of T6 heat-treated Y000 and Y050 alloys. It can be seen from Fig. 8 that phases such as Al, Si, Mg_2Si and Al_3Y are present in A356.2 alloy.

3.3.2 EDS analysis

Typical EDS mapping images of A356.2 alloy with 0.075 wt% Y addition (Y075) after T6 heat treatment are shown in Fig. 9. It is obvious that there mainly exist Al and Si, and a small amount of Mg, Y and Ti. Typical secondary phases shown in zone Y are enlarged to do the elemental mapping, and the results are shown in Fig. 10. Drawing a broken line in the secondary phase across some convex points shown in Fig. 10a, and line scanning is carried out along the given line. The line is enlarged as shown in Fig. 11a, and four convex points are labeled as 1, 2, 3 and 4 located on or near the line. The results of the Al, Si, Mg, Y and Ti line scan are shown in Fig. 11b–f, respectively. It is obvious that the strength of counts per second (CPS) is stronger at the locations close to the convex points (Points

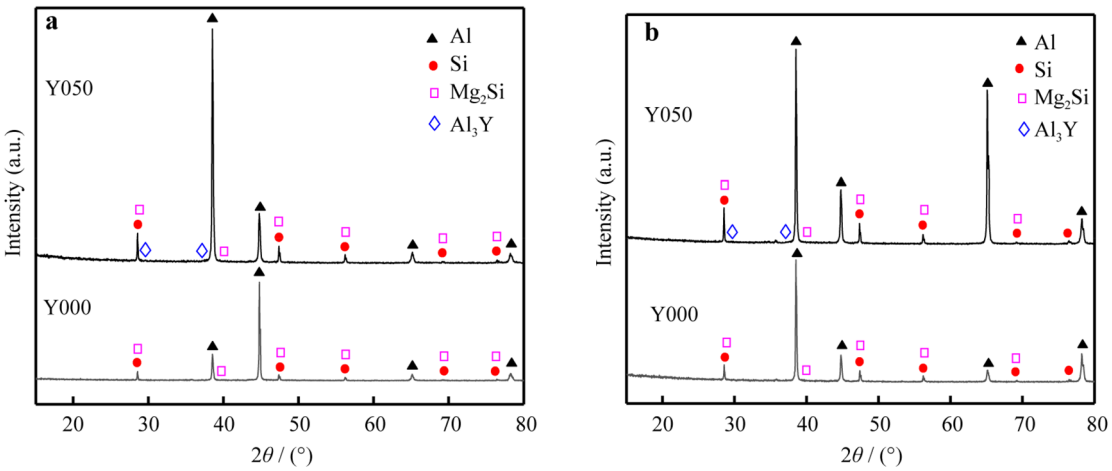

Fig. 8 XRD patterns of Y000 and Y050 A356.2 alloys: **a** as-cast and **b** T6 heat treated

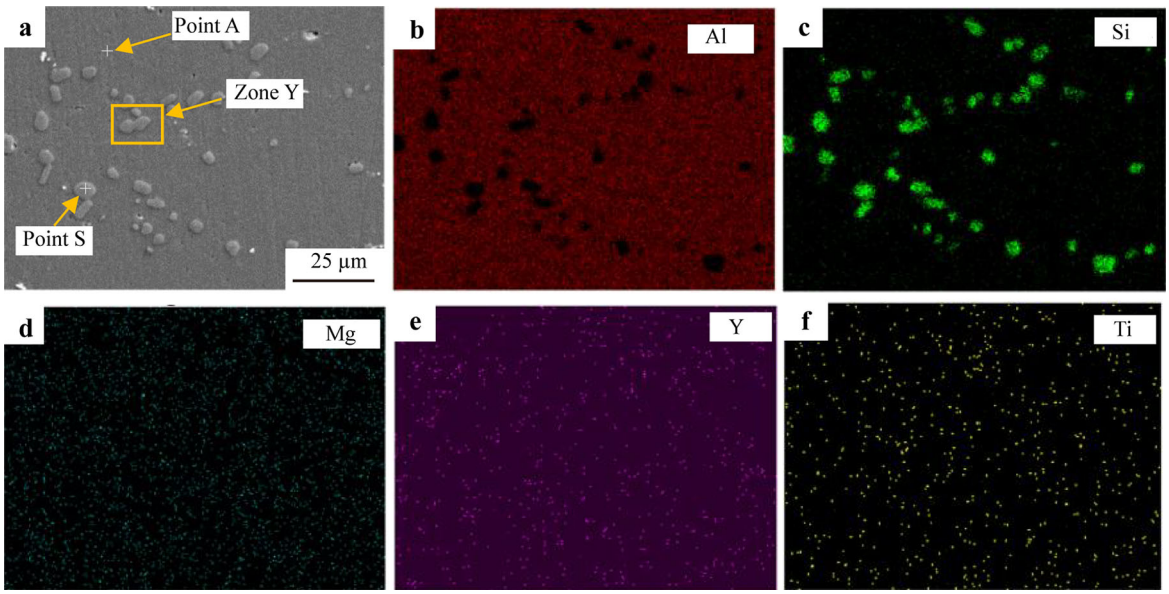

Fig. 9 EDS elemental mapping images of Y075 after T6 heat treatment: **a** scanning zone, **b** Al, **c** Si, **d** Mg, **e** Y and **f** Ti

1–4 in Fig. 11e). This means that the convex points are Y—rich regions, and they are Al_3Y phases.

Two points were analyzed by EDS, as is shown in Fig. 9a labeled as Points A and S. Their main compositions are shown in Table 1. One point lies in α-Al matrix, and another one lies in secondary phase. From Table 1, there is no Y detected in α-Al matrix (Point A); and Si phases and Al_3Y phase are found as the content of Y reaches 0.940 wt%. Based on the EDS line scanning results shown in Fig. 11, those convex points in Figs. 10a, 11a are Al_3Y nano-sized particles. The average diameter of those particles is (104.7 ± 28.9) nm, and the distribution of the grain size is shown in Fig. 12.

3.3.3 DSC analysis

DSC curves of heat-treated A356.2 and 0.075 wt% Y (Y075) optimized samples at the heating and cooling rate of 10 °C·min^{-1} are shown in Fig. 13. There are two obvious exothermic peaks in Fig. 13a and four

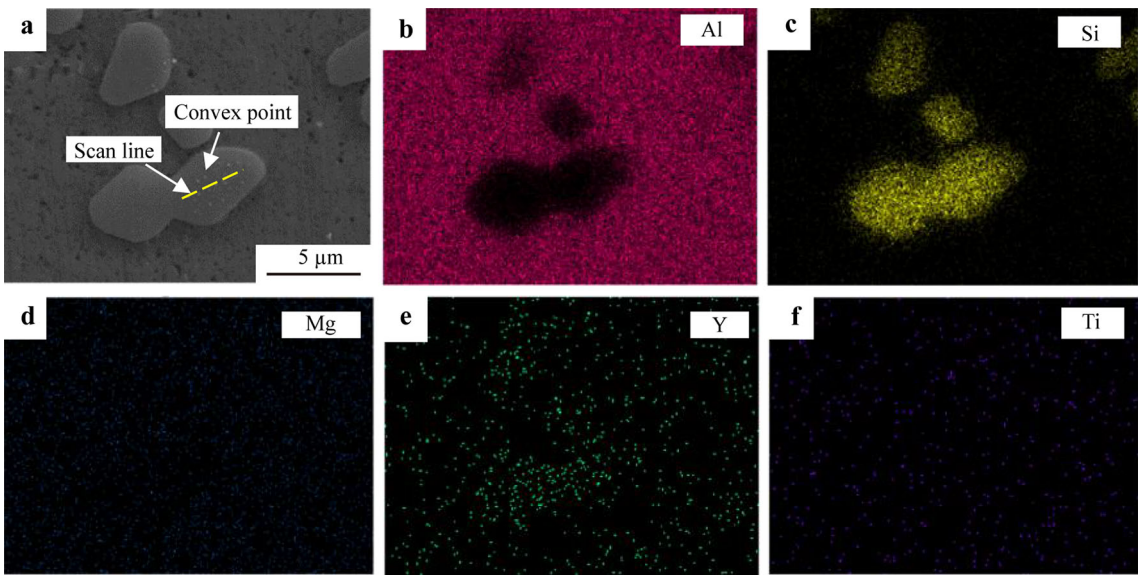

Fig. 10 EDS elemental mapping images of Zone Y in Fig. 9a: **a** scanning zone, **b** Al, **c** Si, **d** Mg, **e** Y and **f** Ti

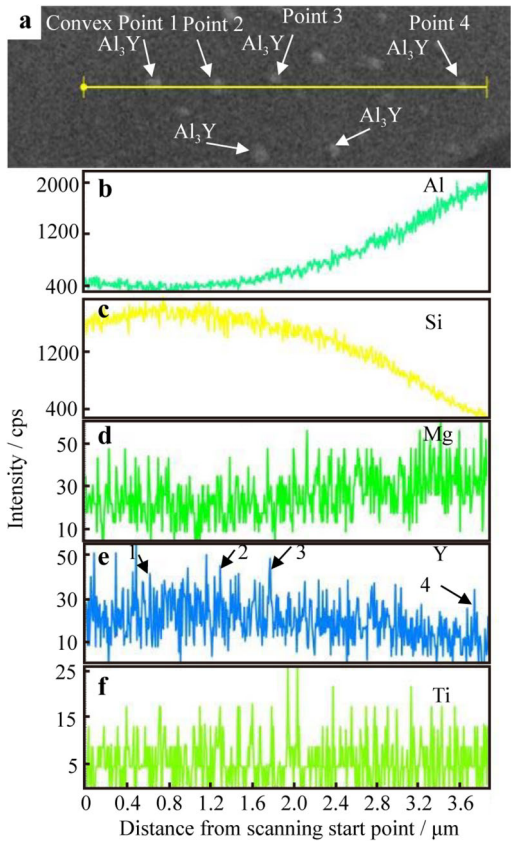

Fig. 11 EDS results of line scanning curves of Y075 after T6 heated: **a** enlarged zone with scanning line, **b** Al, **c** Si, **d** Mg, **e** Y and **f** Ti

endothermic Peaks in Fig. 13b on each curve in the temperature range from 520 to 680 °C, and these peaks indicate specified phase transformations. In details, Peaks P1 and PIV indicate the phase transformations (Liquid $\leftrightarrow \alpha_{Al} + \beta_{Si}$), Peaks P2 and PIII indicate the phase transformations (Liquid $\leftrightarrow \alpha_{Al}$), PII indicates the phase transformations ($\beta_{Al_3Y} \rightarrow \alpha_{Al_3Y}$) and Mg-Si binary eutectic reaction ($Liquid_{1.7\,at\%Si} \rightarrow \alpha_{Mg} + Mg_2Si$), PI indicates the peritectic transformation ($Liquid + \alpha_{Al_3Ti} \rightarrow \alpha_{Al}$). The temperatures of peaks are concluded in Table 2.

From DSC curves shown in Fig. 13a, exothermic peaks P1 and P2 on Y075 curve are 1.1 and 2.3 °C higher than that on Y000 curve, and P1s indicate the eutectic reactions ($\alpha_{Al} + \beta_{Si} \rightarrow$ Liquid) [32]. Compared with the results by Dong et al. [16], because the composition of Al alloy in our work is 0.147 wt% Ti containing A356.2 alloy, which is different from that in Ref. [16], the temperature of eutectic transformation in our work is relatively higher. In addition, the modifier is trace 0.075 wt% Y in this case, versus 0.040 wt% Sr + 0.300 wt% Y in Ref. [16]. According to the DSC curves shown in Fig. 13b, the PIII on Y075 curve is 2.8 °C higher than that on Y000 curve. It could be concluded that the undercooling of the studied A356.2 alloy is increased by 2.8 °C when 0.075 wt% Y is added. The solidification time is shorter with the increase of undercooling, and the SDAS (λ_2) becomes thinner and the microstructure of as-cast A356.2 alloy is refined. This is in good agreement with the results in Fig. 3a. The PIV which indicates the eutectic reactions ($Liquid \rightarrow \alpha_{Al} + \beta_{Si}$) on Y075 curve is 2.3 °C higher than that on Y000 curve.

The secondary phases in A356.2 are various and different. In our experiments and discussions above, they are Si, Mg_2Si and Al_3Ti. Because of the exist of impurity Fe, some Fe rich phases such as Al_5FeSi [2, 4, 5, 33] also exist. When Y is added, Al_3Y and Al_2Y exist accordingly. However, some secondary phases such as Al_3Y_2Si [16] may also exist. Actually, they are difficult to be distinguished and determined except matrix α-Al and eutectic Si phases. However, eutectic Si, α-Al, Mg_2Si, Al_3Y are determined according to the EDS and XRD results from Refs. [2, 21, 22] and experiments in this work.

It is well known that Mg_2Si plays an important role in improving the strength of Al-Si alloy. The melting point of pure Mg_2Si is 1085 °C, and the eutectic reaction $Liquid_{1.7\,at\%Si} \rightarrow \alpha_{Mg} + Mg_2Si$ occurs at 637.6 °C according the Mg-Si phase diagram. In the as-cast A356.2 alloy, undissolved solid Mg_2Si appears in the boundary of α-Al matrix in blocky morphology [26]. In the stage of solutionizing during T6 heat treatment, this blocky Mg_2Si becomes smaller, and some can be dissolved completely. In the stage of artificial aging in T6 heat treatment, some small Mg_2Si particles are precipitated with the solubility decrease in α-Al and Si phase.

Al_3Y is a new phase due to Y addition. According to Al-Y phase diagram and well-known level rule, the weight ratio of (Al_3Y)/(α-Al) in Y075 here is 0.0014. This value is very small. Actually, Al_3Y is always accompanied with other secondary phases and it is identified in this work, as

Table 1 Compositions analysis of points labeled in Fig. 9a

Point	Al		Si		Mg		Y		Ti		Phases indicated
	w/wt%	*x*/at%	*w*/wt%	*x*/at%	*w*/wt%	*x*/at%	*w*/wt%	*x*/at%	*w*/wt%	*x*/at%	
A	98.15	98.28	1.38	1.33	0.24	0.27	0	0	0.22	0.12	α-Al
S	7.73	8.07	91.19	91.50	0.08	0.09	0.94	0.30	0.06	0.04	Si + Al_3Y

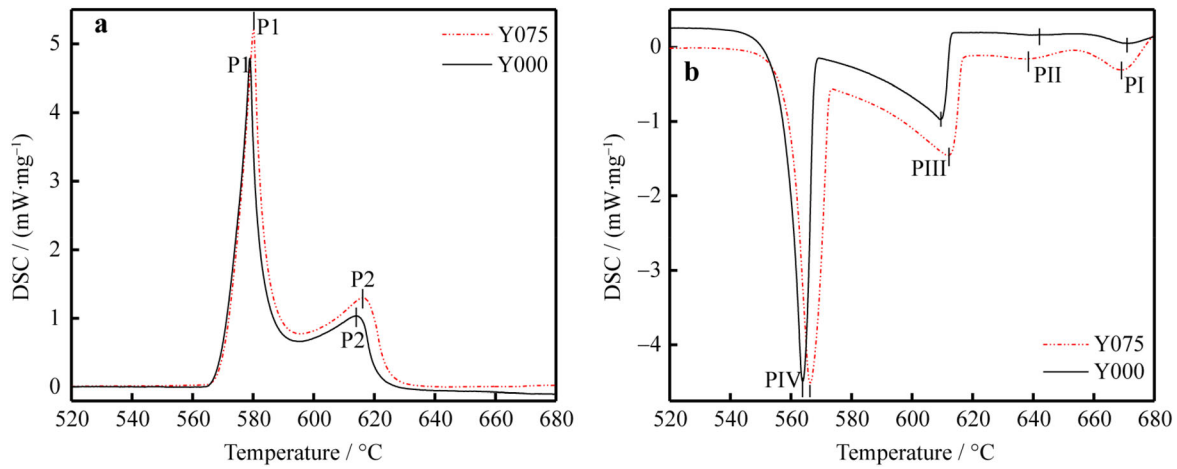

Fig. 13 DSC curves of T6 heat-treated A356.2 Y000 and Y075 specimens: **a** heating at 10 °C·min^{-1} and **b** cooling at 10 °C·min^{-1}

Table 2 Temperature of peaks on DSC curves in Fig. 13 (°C)

Alloy	P1	P2	PI	PII	PIII	PIV
Y000	579.0	614.1	670.9	639.6	609.1	563.9
Y075	580.1	616.4	669.2	637.1	611.9	566.2

shown in Fig. 11a. XRD results shown in Fig. 8 and DSC results shown in Fig. 13 help to support the identification here. This is also consistent with research works from Refs. [22, 26].

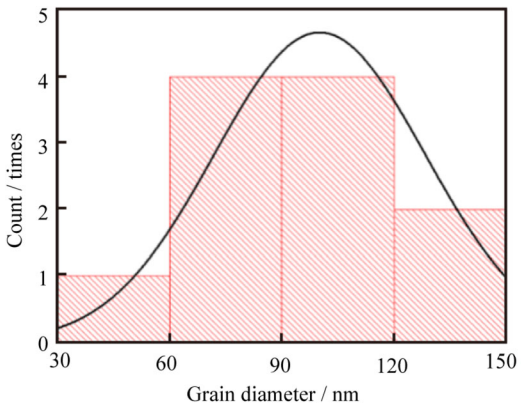

Fig. 12 Histogram of diameter distribution of Al_3Y particles in Fig. 11a

4 Conclusion

In this work, the effects of yttrium microalloying (up to 0.100 wt%) on microstructure refinement and mechanical properties of A356.2 alloy were investigated. The microstructure evolution and mechanical properties of A356.2 aluminum alloy under as-cast and T6-treated conditions were analyzed. It is found that the strength of as-cast A356.2 alloy obeys the Hall–Petch equation, and the fitting relationship between the yield strength and grain size is $YS = -354.1 + 2875d^{-1/2}$ with a correlation of $R^2 = 0.83$. When 0.050 wt% of Y was added, it achieved the optimum values of the YS, UTS and El after T6 treated. The results show an increase of 218%, 77% and 155% in YS, UTS and EI, respectively, in comparison to those of the as-cast A356.2.

The temperature of eutectic reactions (Liquid $\rightarrow \alpha_{Al} + \beta_{Si}$) is increased by 2.3 °C when 0.075 wt% Y is added compared with no Y added A356.2. When yttrium is added, the undercooling is increased; the SDAS ($\lambda 2$) and the microstructure of as-cast A356.2 alloy are refined. After T6 heat treatment, the strength of A356.2 is improved significantly. Mg_2Si precipitates are dispersed in α-Al matrix, and nano-sized Al_3Y particles with average diameter of (104.7 ± 28.9) nm precipitate on the surface of the Si phase.

Acknowledgments This study was financially supported by the National Natural Science Foundation of China (No. 51601102), the Natural Science Foundation of Shandong Province (No. ZR2016EEM48) and the Key Research and Development Program Plan of Shandong Province (No. 2018GGX103012).

References

[1] Yang CC, Liu ZW, Zheng QL, Cao YL, Dai XH, Sun L, Zhao JR, Xing JD, Han QY. Ultrasound assisted in-situ casting

technique for synthesizing small-sized blocky Al_3Ti particles reinforced A356 matrix composites with improved mechanical properties. J Alloys Compd. 2018;747:580.
[2] Ram SC, Chattopadhyay K, Chakrabarty I. Microstructures and high temperature mechanical properties of A356-Mg_2Si functionally graded composites in as-cast and artificially aged (T6) conditions. J Alloys Compd. 2019;805:454.
[3] Xie HJ, Cheng YL, Li SX, Cao JH, Cao L. Wear and corrosion resistant coatings on surface of cast A356 aluminum alloy by plasma electrolytic oxidation in moderately concentrated aluminate electrolytes. Trans Nonferrous Met Soc China. 2017;27(2):336.
[4] Kittisak C, Ussadawut P, Sindo K, Chaowalit L. Mechanical properties of squeeze-cast Al-7Si-0.3Mg alloys with Sc-modified Fe-rich intermetallic compounds. Rare Met. 2018;37(9):769.
[5] Jiang B, Ji ZS, Hu ML, Xu HY, Xu S. A novel modifier on eutectic Si and mechanical properties of Al-Si alloy. Mater Lett. 2019;239:13.
[6] Tsai YC, Chou CY, Lee SL, Lin CK, Lin JC, Lim SW. Effect of trace La addition on the microstructures and mechanical properties of A356 (Al-7Si-0.35Mg) aluminum alloys. J Alloys Compd. 2009;487(1–2):157.
[7] Lin GY, Li K, Feng D, Feng YP, Song WY, Xiao MQ. Effects of La-Ce addition on microstructure and mechanical properties of Al-18Si-4Cu-0.5Mg alloy. Trans Nonferrous Met Soc China. 2019;29(8):1592.
[8] Cheng CX, Yang XJ, He Y, Zhu YB. The properties of A356 aluminum alloy with Ce addition and its refining mechanism. Chinese J Rare Met. 2018;42(11):1127.
[9] Torre EAD, Bustamante RP, Cisneros JC, Esparze CDG, Prieto HMM, Sanchez RM. Mechanical properties of the A356 aluminum alloy modified with La/Ce. J Rare Earth. 2013;31(8):811.
[10] Hu Z, Yan H, Rao YS. Effects of samarium addition on microstructure and mechanical properties of as-cast Al-Si-Cu alloy. Trans Nonferrous Met Soc China. 2013;23(11):3228.
[11] Liu WY, Xiao WL, Xu C, Liu MW, Ma CL. Synergistic effects of Gd and Zr on grain refinement and eutectic Si modification of Al-Si cast alloy. Mater Sci Eng A. 2017;693:93.
[12] Chen ZW, Ma CY, Chen P. Modifying agent selection for Al-7Si alloy by Miedema model. Int J Miner Metall Mater. 2012;19(2):131.
[13] Liu Z, Hu YM. Effect of yttrium on the microstructure of a semi-solid A356 Al alloy. Rare Met. 2008;27(5):536.
[14] Xu C, Ma CL, Sun YF, Hanada SJ, Lu GX, Guan SK. Optimizing strength and ductility of Al-7Si-0.4Mg foundry alloy: role of Cu and Sc addition. J Alloys Compd. 2019;810:151944.
[15] Li QL, Li BQ, Li JB, Zhu YQ, Xia TD. Effect of yttrium addition on the microstructures and mechanical properties of hypereutectic Al-20Si alloy. Mater Sci Eng A. 2018;722:47.
[16] Dong Y, Zheng RG, Lin XP, Ye J, Sun L. Investigation on the modification behavior of A356 alloy inoculated with a Sr-Y composite modifier. J Rare Earth. 2013;31(2):204.
[17] Rao AKP, Das K, Murty BS, Chakraborty M. Microstructural features of as-cast A356 alloy inoculated with Sr, Sb modifiers and Al-Ti-C grain refiner simultaneously. Mater Lett. 2008;62(2):273.
[18] Zhang X, Huang LK, Zhang B, Chen YZ, Duan SY, Liu G, Yang CL, Liu F. Enhanced strength and ductility of A356 alloy due to composite effect of near-rapid solidification and thermo-mechanical treatment. Mater Sci Eng A. 2019;753:168.
[19] Mahmoud MG, Elgallad EM, Ibrahim MF, Samuel FH. Effect of rare earth materials on porosity formation in A356 alloy. Int J Metalcast. 2018;12(2):251.
[20] Hu XP, Zhao Y, Wang Q, Zhang XZ, Li RX, Zhang BR. Effect of pouring and cooling temperatures on microstructures and mechanical properties of as-cast and T6 treated A356 alloy. China Foundry. 2019;16(6):380.
[21] Mao GL, Yan H, Zhu CC, Wu Z, Gao WL. The varied mechanisms of yttrium (Y) modifying a hypoeutectic Al-Si alloy under conditions of different cooling rates. J Alloys Compd. 2019;806:909.
[22] Wei ZF, Lei YS, Yan H, Xu XH, He JJ. Microstructure and mechanical properties of A356 alloy with yttrium addition processed by hot extrusion. J Rare Earth. 2019;37(6):659.
[23] Zhang YZ, Gu J, Tian Y, Gao HY, Wang J, Sun BD. Microstructural evolution and mechanical property of Al-Zr and Al-Zr-Y alloys. Mater Sci Eng A. 2014;616:132.
[24] Hu JL, Bo H, Liu LB, Jin ZP. Thermodynamic study of the Al-Sc-Y system. Thermochimi Acta. 2018;661:147.
[25] Wu DY, Kang J, Feng ZH, Su R, Liu CH, Li T, Wang LS. Utilizing a novel modifier to realize multi-refinement and optimized heat treatment of A356 alloy. J Alloys Compd. 2019;791:628.
[26] Li QL, Li BQ, Liu JJ, Li JB, Liu DX, Lan YF, Xia TD. Modification of hypereutectic Al-20 wt% Si alloy based on the addition of yttrium and Al-5Ti-1B modifiers mixing melt. Int J Metalcast. 2019;13:367.
[27] Dang B, Liu CC, Liu F, Liu YZ, Li YB. Effect of as-solidified microstructure on subsequent solution-treatment process for A356 Al alloy. Trans Nonferrous Met Soc China. 2016;26(3):634.
[28] Milkerelt B, Wanderka N, Schick C, Kessler O. Continuous cooling precipitation diagrams of Al-Mg-Si alloys. Mater Sci Eng A. 2012;550:87.
[29] Dorin T, Ramajayam M, Babaniaris S, Jiang L, Langan TJ. Precipitation sequence in Al-Mg-Si-Sc-Zr alloys during isochronal aging. Materialia. 2019;8:100437.
[30] Jian SY, Wang RH. Grain size-dependent Mg/Si ratio effect on the microstructure and mechanical/electrical properties of Al-Mg-Si-Sc alloys. J Mater Sci Technol. 2019;35(7):1354.
[31] Ma GH, Li RD, Li RX. Effect of Mg_2Si particles on low-temperature fracture behavior of A356 alloy. Mater Sci Eng A. 2016;674:666.
[32] Wang QG, Davidson CJ. Solidification and precipitation behaviour of Al-Si-Mg casting alloys. J Mater Sci. 2001;36:739.
[33] Asgar G, Peng LM, Fu PH, Yuan LY, Liu Y. Role of Mg_2Si precipitates size in determining the ductility of A357 cast alloy. Mater Design. 2020;186:108280.